Ti$_3$O$_5$ and Al$_2$TiO$_5$ Crystals Flotation Characteristics from Ti-bearing Blast Furnace Slag: A Density Functional Theory and Experimental Study

Shan Ren [1],*, Zenghui Su [2], Weizao Liu [2], Yali Sun [1], Xiaoming Li [3] and Jian Yang [1]

[1] College of Materials Science and Engineering, Sichuan University of Science & Engineering, Zigong 643000, China; sonaly@126.com (Y.S.); skyinjune@cqu.edu.cn (J.Y.)

[2] College of Materials Science and Engineering, Chongqing University, Chongqing 400044, China; suzenghui@cqu.edu.cn (Z.S.); liuwz@cqu.edu.cn (W.L.)

[3] School of Metallurgical Engineering, Xi'an University of Architecture and Technology, Xi'an 710055, China; xmli88@126.com

* Correspondence: shan.ren@cqu.edu.cn

Abstract: Anosovite crystalline is an ideal mineral for flotation from the Ti-bearing blast furnace (TBBF) slag. Ti$_3$O$_5$ crystal and Al$_2$TiO$_5$ crystal are two kinds of anosovites, and the Al element significantly affects the electronic structure and flotation performance of anosovite. The floatability of Ti$_3$O$_5$ and Al$_2$TiO$_5$ crystals were studied by Mulliken populations, energy bands, and density of states (DOS). In addition, the flotation experiment of the two kinds of anosovite crystals (Ti$_3$O$_5$ and Al$_2$TiO$_5$) was conducted and proved that the density functional theory (DFT) calculation results were accurate. Compared with Ti$_3$O$_5$ crystal, the Fermi energy level of Al$_2$TiO$_5$ crystal shifts around 2 eV in a negative direction by DOS analysis, which is beneficial to flotation. And Al$_2$TiO$_5$ crystal possesses a larger value of bond population, which is 0.41, for Ti-O bonds than Ti$_3$O$_5$ crystal and the bond length of Ti-O in Al$_2$TiO$_5$ crystal is shorter, therefore Al$_2$TiO$_5$ crystal shows a stronger covalency. The changes of the Fermi energy level and the covalency bonds in Al$_2$TiO$_5$ crystal both demonstrated that doping the Al component into the Ti$_3$O$_5$ crystal was beneficial to improve the flotation effect. Moreover, the Al$_2$TiO$_5$ crystal had a higher flotation efficiency compared to the Ti$_3$O$_5$ crystal when the dosages of salicylhydroxamic acid (SHA) and sodium oleate were the same. Therefore, both DFT calculation and experiment show that the flotation effect of the Al$_2$TiO$_5$ crystal is better than that of the Ti$_3$O$_5$ crystal.

Keywords: Ti$_3$O$_5$ crystal; Al$_2$TiO$_5$ crystal; DFT; flotation

1. Introduction

In southwest of China, there is a large amount of high Ti-bearing vanadium-titanomagnetite and most of which is used for ironmaking process in blast furnace. Therefore, Ti-bearing blast furnace (TBBF) slag is becoming one of the most important secondary resources of titanium, which contains approximately 20–26% TiO$_2$ [1–4]. However, titanium is difficult to separate and utilize due to its dispersity in different fine minerals (about 10 μm). Some researchers [5,6] chose perovskite (CaTiO$_3$) as a Ti enrichment phase for the separation of titanium element. In theory, the amount of TiO$_2$ in perovskite is about 59%, with a density similar to the glassy phase in the slag, so separating and extracting Ti is difficult from perovskite phase in TBBF slag [7,8]. Compared with perovskite, anosovite crystal contains more than 70% TiO$_2$ (M$_x$Ti$_{3-x}$O$_5$ and $0 \leq x \leq 2$, where M represents the divalent Mg, Fe, Ti or trivalent Ti, Fe, Al, etc.) with a density (4.20 g/cm^{-3}) significantly higher than that of glass

phase (2.81 g/cm^{-3}) [7]. Therefore, anosovite crystal may be a better alternative for recovering titanium from TBBF slag.

In our previous research [9–16], Ti-bearing ore sintering and Ti-bearing slag characteristics were studied systematically. B_2O_3 was chosen as the modifier for obtaining the Ti-rich phases, and the results showed that the rise of the (Mg + Al)/(Ca + Si) ratio and B_2O_3 in slag were beneficial to form $[TiO_6]^{8-}$ octahedral units and thus beneficial to the precipitation of anosovite from the TBBF slag [14,15]. In addition, Anosovite was successfully obtained from TBBF slag, and the lower cooling temperature and extension of the holding time promoted the coarsening of anosovite crystals [16].

Floatation technology has been applied maturely for mineral separation, and its cost is low. The separation of anosovite crystal from the gangue minerals by flotation is influenced by the electronic structures of mineral crystals [17,18], and the floatability of each mineral is closely related to their electronic structure. Mg and Al had positive effects on the stability of Ti_3O_5 crystal structure [15], whereas experimental methods were challenging to explain the microscopic mechanisms of this phenomenon [19]. Density functional theory (DFT) [20,21], widely and successfully applied in simulations throughout engineering and sciences, a supplement of modern experimental methods, can be used to analyze mineral crystal structures from atom and electron aspects [22]. Related research was conducted on magnesium-bearing anosovite floatation from Ti-bearing electric slag, and the results showed that Mg entering the Ti_3O_5 lattice changed the crystal and electronic structures of Ti_3O_5. Changes in the electronic structures of minerals are bound to affect the adsorption of reagents on the surfaces, which caused the appearance of defects in the crystalline Ti_3O_5 and change the flotability of minerals, which was beneficial to floatation [23]. However, besides the magnesium element, there was a certain content of aluminum in the TBBF slag [14–16], which may affect the crystalline structure of Ti_3O_5 crystal. Still, the flotation of anosovite crystals from Ti-bearing blast furnace slag is still not reported in the literature.

Therefore, the electronic structures of Ti_3O_5 and Al_2TiO_5 crystals were calculated by DFT, and the influence of Al element on crystal structures of Ti_3O_5 was studied. In addition, the calculation results were compared with flotation experiment results. and the DFT calculation results provide clarification of the experimental results. It is expected that theoretical support for the separation process of TBBF slag through flotation aluminum-bearing anosovite crystal can be established.

2. Experimental

2.1. Materials

The single mineral sample of anosovite (Ti_3O_5) crystal was obtained from titanium production in Sichuan province in China, and its purity was up to 97.12%, with only small amount of Al_2O_3, MgO, Cr, etc. dissolve in it. Tt is therefore marked as Ti_3O_5 crystal and used for the flotation experiment. Besides, the anosovite crystal was doped with aluminum, and the chemical composition is mainly Al_2TiO_5, the purity of which is 92.63%. Ti_3O_5 and Al_2TiO_5 crystals (each 4 g) were used as raw materials for the flotation experiments in this study.

2.2. Analysis and Experiment Method

2.2.1. Construction Analysis of Ti_3O_5 and Al_2TiO_5 Crystalline Models

DFT is a high-precision quantum chemical calculation tool that uses electron density instead of wave function as the research object. The Cambridge Sequential Total Energy Package (CASTEP) module in Materials Studio software [24,25] is on the basis of the theory of plane wave pseudopotential and the number and type of atoms can be used to predict and calculate the crystal lattice parameters, band structure, solid density, charge density and wave function. The interaction between ionic core and valence electrons was described using the Ultra-soft pseudopotentials [26]. The selected valence electron configurations in this study were $Ti3s^23p^63d^24s^2$, $Al3s^23p^1$, and $O2s^22p^4$. Furthermore, the sampling

accuracy of the Brillouin zone was defined by a $2 \times 2 \times 1$ k-point set. The Pulay density mixing method (PDMM) is used for self-consistent electronic minimization, in which the convergence tolerance energy and maximum force tolerance on each atom was set to 1.0×10^{-6} eV/atom and 1.0×10^{-2} eV/Å for the energy calculation.

The crystal structure diagrams of Ti_3O_5 [23] and Al_2TiO_5 formed after the solid solution of Al into Ti_3O_5 crystals were shown in Figure 1. Relevant research results showed that Al-O bond and Ti-O bond with stronger covalency existed in Al_2TiO_5 crystal formed after the solid solution of Al into Ti_3O_5 crystal, which was more stable than Ti_3O_5 crystal [22]. Both crystal Ti_3O_5 and Al_2TiO_5 belong to the orthorhombic with space group Cmcm. The lattice parameters a, b, and c of Ti_3O_5 are 9.84, 3.76, and 9.86 nm, respectively, which for the Al_2TiO_5 crystal are 9.84, 3.76, and 9.861 nm, respectively. The lattice parameters α, β, and γ of Ti_3O_5 and Al_2TiO_5 are 90°.
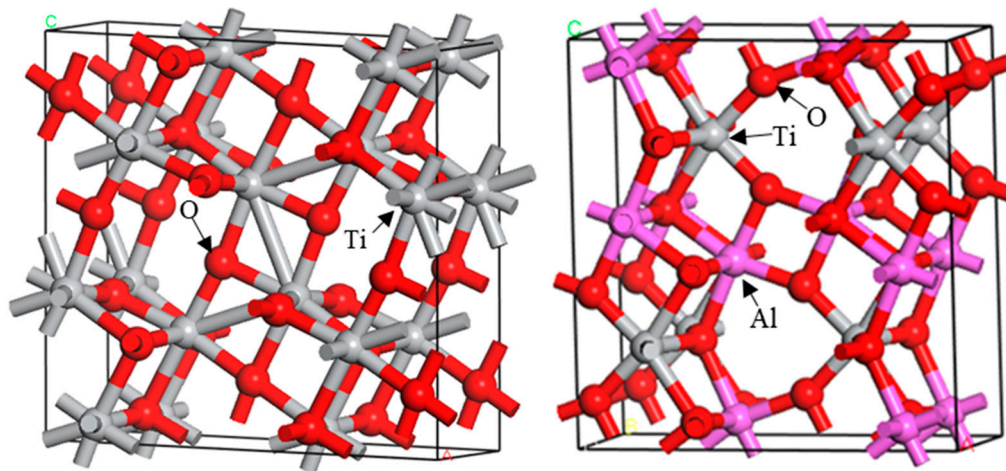

Figure 1. Crystal cell models of Ti_3O_5 [23] and Al_2TiO_5.

2.2.2. Flotation Experimental

The flotation behavior of anosovite crystal was carried out in a small hanging laboratory flotation machine with an effective volume of 60 mL and an impeller speed of 1900 r/min. The water in flotation process was deionized water. The test procedure was as follows: 4 g of anosovite sample with a particle size of about 180 mesh was placed in a 60 mL flotation cell. Then, the collector and frother were introduced in the flotation machine and then stirred for 2 min and 3 min, respectively. Finally, the flotation pulp scraped for 4 min. The pH adjuster was hydrochloric acid and sodium hydroxide, and the test temperature was 20 ± 5 °C. After collecting and drying, the recovery of the product was calculated.

3. Results and Discussion

3.1. Energy Bond Structures of Ti_3O_5 and Al_2TiO_5 Crystals

Figures 2 and 3 show the band structure of two different anosovites of Ti_3O_5 and Al_2TiO_5. The Fermi energy level is uniformly used as the energy zero point in the Figure 2. It can be seen intuitively that the energy band of Ti_3O_5 is divided into five parts from −60 eV to 10 eV.
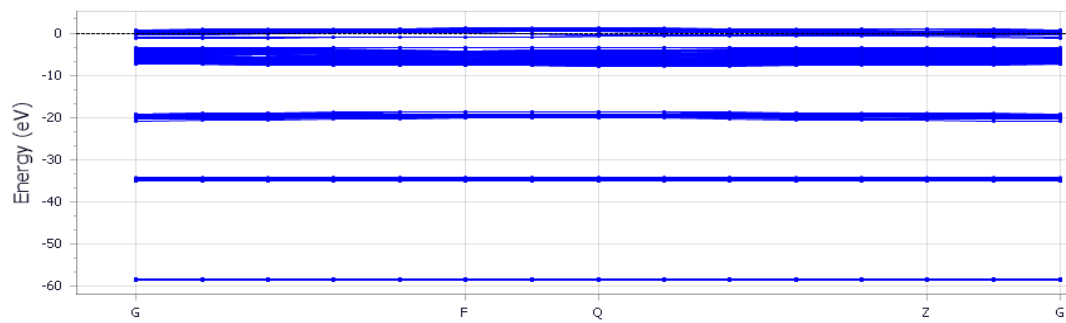
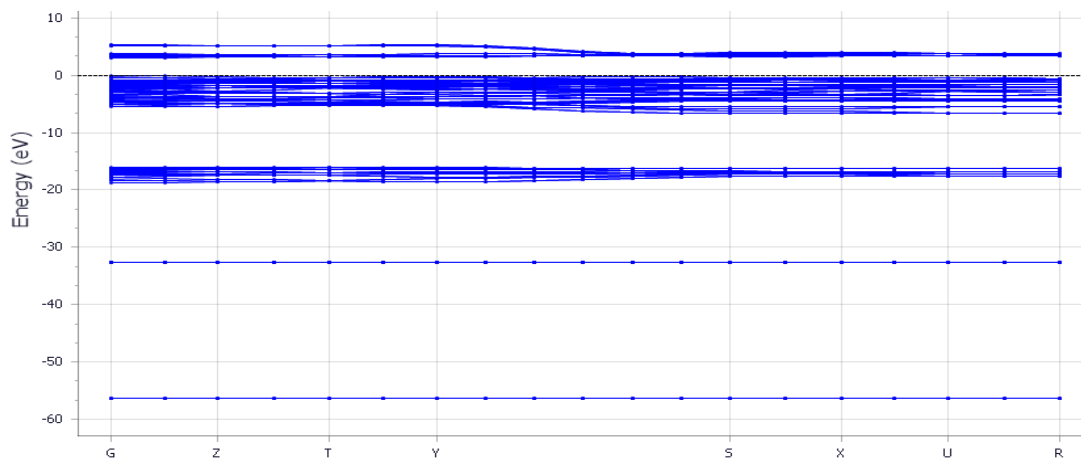**Figure 2.** Energy band structure of Ti_3O_5 crystal.

Figure 3. Energy band structure of Al_2TiO_5 crystal.

From Figure 3, there are five parts for the valence band of Al_2TiO_5 crystal, and the band structure of Al_2TiO_5 is relatively close to that of Ti_3O_5. This may be due to the same valency of Al^{3+} and Ti^{3+}, so Al entering into Ti_3O_5 crystal has relatively little impact on its energy band structure. However, the energy of all Al_2TiO_5 band increased about 2 eV compared with that of Ti_3O_5, indicating that he valence and conduction bands have increased in energy. Moreover, the anions adsorption on the surface of minerals is promoted by the movement of Fermi energy level and thus the adsorption probability increases [27]. Therefore, the adsorption of anosovite on the mineral surface is affected by the site of the Fermi energy level. Changes in the electronic structures of minerals are bound to affect the adsorption of reagents on the surfaces, which change the flotability of minerals. A decrease in the Fermi level may result in an increase in the number of holes on the surface of the Al_2TiO_5, which in turn may increase the adsorption or adsorption rate of the anion collector on the crystal during the flotation process, as well as the adsorption stability, which is conducive to the flotation process [28,29]. Therefore, doping Al component into Ti_3O_5 should be beneficial to improve the flotation effect.

3.2. DOS Distributions of Ti_3O_5 and Al_2TiO_5 Crystals

The distributions of electronic DOS of Ti_3O_5 and Al_2TiO_5 crystals are shown in Figures 4 and 5. From Figure 4, the valence band of Ti_3O_5 consists of five parts.
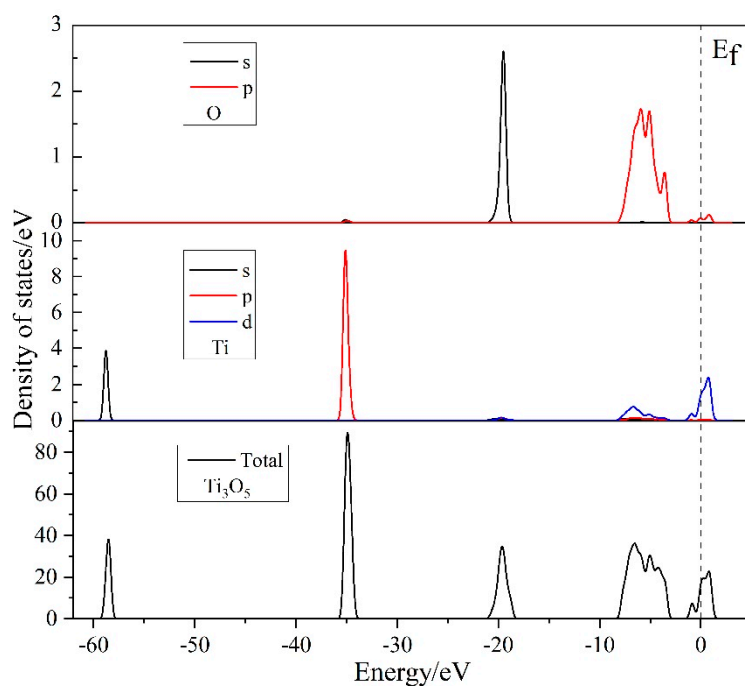
Figure 4. Total and partial density of states (DOS) of the Ti_3O_5 crystal.
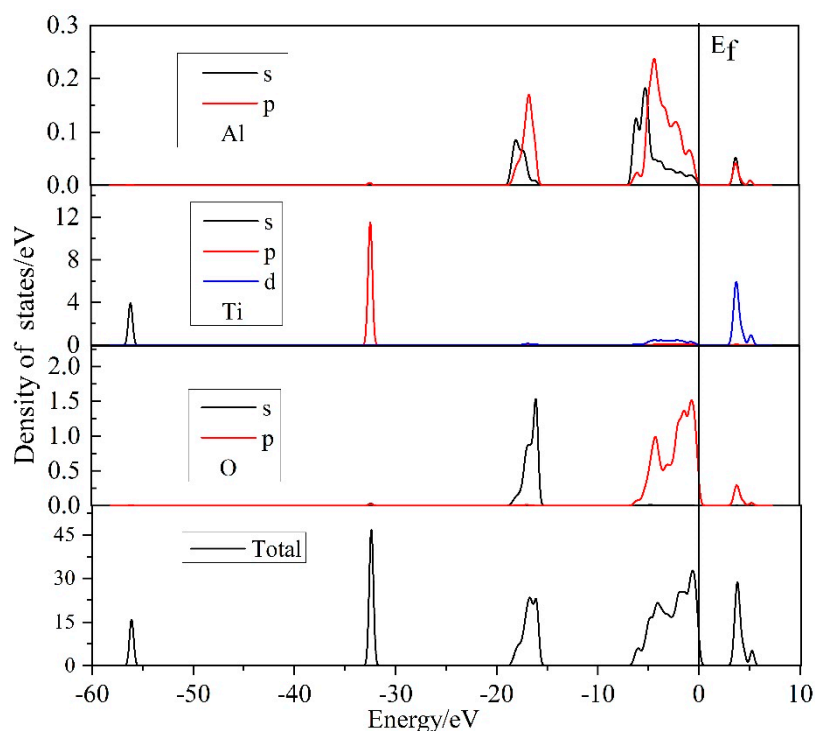

Figure 5. Total and partial DOS of the Al_2TiO_5 crystal.

From the DOS of each atom, it can be seen that the valence band peak for Ti_3O_5 crystal at approximately −59.1 eV, which is attributed to orbit Ti4s electrons. Moreover, almost the entire valence band peak at −35.0 and −20.0 eV come from Ti3p orbit and O2s orbit electrons, respectively. The above-mentioned valence bands are all with very sharp peaks and narrow energy bands, which show that the electron is distributed comparatively locally. The electronic peak ranged from −8.0 to -4.0 eV is contributed the O2p and part of Ti3p and Ti3d orbit. The O2p orbit exhibits a very high electronic peak

due to the strong localization of electron in the orbit. The overlap of the electronic peaks of the O2p and Ti3d orbit at −8.0 ~ 4.0 eV, and the Fermi energy level indicates that electrons of the Ti3d to O2p orbit have a transition phenomenon and can interact with each other. The results are consistent with Wang et al [23]. There are some changes in the valence band of Ti_3O_5 after Al entering Ti_3O_5 lattice. From Figure 5, Al3s and Al3p orbits appear on the peaks of Al_2TiO_5 valence band at about −18, −6, and −0 eV and the Fermi energy level. Therefore, in addition to the contribution of Ti3d and O2p orbits, the valence band peak at the Fermi energy level of Al_2TiO_5 crystal also comes from Al3s and Al3p orbits. Moreover, the electronic peaks of the O2p, Ti3d, Al3s, and Al3p orbit overlap at the Fermi energy level, demonstrating that they can interact with each other.

3.3. Distributions of Ti_3O_5 and Al_2TiO_5 Atomic Charges

The distributions of electronic states of atoms were from Mulliken population analysis. The valence electrons distributed around atoms are known as atom populations and the overlapped electron charges distributed between two atoms are called bond populations. With the help of Mulliken population analysis [30–33], the charge distribution, transfer distribution and bonding between atoms can be understood.

Table 1 is the calculation results of the Mulliken population analysis of Ti_3O_5 crystal, which is similar to Wang et al. [23]. It can be seen from the average charge of the atom that the electrons number in the Ti atom is 10.87e and lost 1.12e, which indicated that the Ti in Ti_3O_5 crystal is a donor of electrons. Meanwhile, the number of electrons localized on the O atom is 6.67e and obtained 0.67e, indicating that O is acceptor of electrons. Besides, the calculation of Mulliken populations of Ti–O bonds in Ti_3O_5 crystal shows that the value of bond population for Ti–O is 0.367 and the bond length is 2.038 Å. Therefore, the Ti–O bond inside the Ti_3O_5 crystal is covalent, which has directionality, saturation and certain hydrophilicity.

Table 1. Average Mulliken populations of atoms in Ti_3O_5 crystal.

Species	Atomic Populations (Mulliken)			Total/e	Charge/e
	s	p	d		
O	1.84	4.83	0	6.67	−0.67
Ti	2.26	6.31	2.30	10.87	+1.12

Tables 2 and 3 are the calculation results of the Mulliken population analysis of Al_2TiO_5 crystal. It can be seen that Ti and Al lose 1.39 e and 1.63 e, respectively, so the Ti and Al have 1.39 e and 1.63 e charges, respectively. O obtained 0.93e and have the −0.93 e of charges. The value of population and length for Ti-O bond in Al_2TiO_5 crystal are 0.41 e and 1.98 Å, respectively, while that of Al-O in Al_2TiO_5 crystal are 0.46 Å and 1.85 Å, respectively.

Table 2. Average Mulliken populations of atoms in Al_2TiO_5 crystal.

Species	Atomic Populations (Mulliken)			Total	Charge
	s	p	d		
O	1.85	5.08	0	6.93	−0.93
Al	0.51	0.87	0	1.38	+1.63
Ti	2.22	6.22	2.17	10.61	+1.39

Table 3. Mulliken populations of bonds in Al_2TiO_5 crystal.

Bond	Population (e)	Length (Å)
Ti-O	0.41	1.98
Al-O	0.46	1.85

Compared with Ti_3O_5 crystal, O atom obtains more electrons in Al_2TiO_5 crystal because Ti atom gets electrons more easily than Al atom. From Tables 1 and 2, O atom in Ti_3O_5 and Al_2TiO_5 crystals obtains 0.67 and 0.93 electrons, respectively. Moreover, Al_2TiO_5 crystal possesses a larger value of bond population for Ti–O than Ti_3O_5 and the bond length of Ti–O in Al_2TiO_5 crystal is shorter compared with Ti_3O_5; therefore, the covalency of crystalline Al_2TiO_5 is stronger than Ti_3O_5. In addition, compared with the Ti–O bond, the value of bond population for Al–O is larger, which indicates that the covalency of Al-O bond in the Al_2TiO_5 crystal is greater than that of the Ti–O bond.

3.4. Flotability of Ti_3O_5 and Al_2TiO_5 Crystals

The electron structures of anosovite crystalline display obvious difference between Ti_3O_5 and Al_2TiO_5 crystal for the doping of aluminum into Ti_3O_5 crystal. In addition, they have a significant difference on the chemical compositions, so it is reasonable to assume that the flotabilities of Ti_3O_5 and Al_2TiO_5 crystal is different. Therefore, the flotation experiments on the Ti_3O_5 and Al_2TiO_5 crystals used sodium oleate, SHA were conducted, and the experiment results are given in Figures 6 and 7. When the dosage of sodium oleate was 8.0×10^{-5} mol/L, the recovery rate of Ti_3O_5 crystal reaches the highest value of 72.21%, while that of Al_2TiO_5 crystal reaches the maximum value of 79.24%. When using SHA as collectors, the best recovery rate of Ti_3O_5 and Al_2TiO_5 crystals were 80.12% and 84.15%, respectively. For comparison [34], the anosovite of $Mg_{0.09}Ti_{2.9}1O_5$ from Ti-bearing electric slag has a higher recovery, which can reach a maximum recovery of 93.26% at an SHA dosage of 4×10^{-5} mol/L. It can be seen from Figures 6 and 7 that the recovery rate of anosovite crystal is higher when SHA is used as the collector, indicating that sodium oleate had a stronger ability to capture anosovite. More importantly, the recovery rate of Al_2TiO_5 crystal has a higher recovery rate compared with Ti_3O_5 crystal when the flotation conditions are the same. Therefore, doping the Al component into the Ti_3O_5 crystal should be beneficial to improve the flotation effect from TBBF slag.
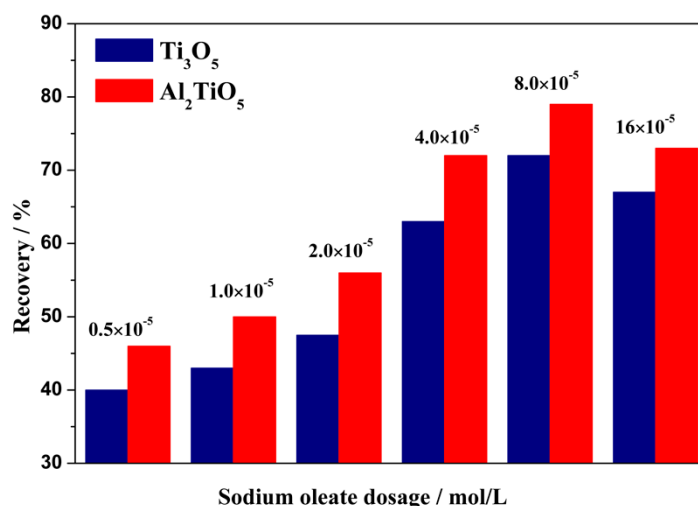

Figure 6. Dosage effect of sodium oleate on flotability of Ti_3O_5 and Al_2TiO_5 crystals (pH = 6).
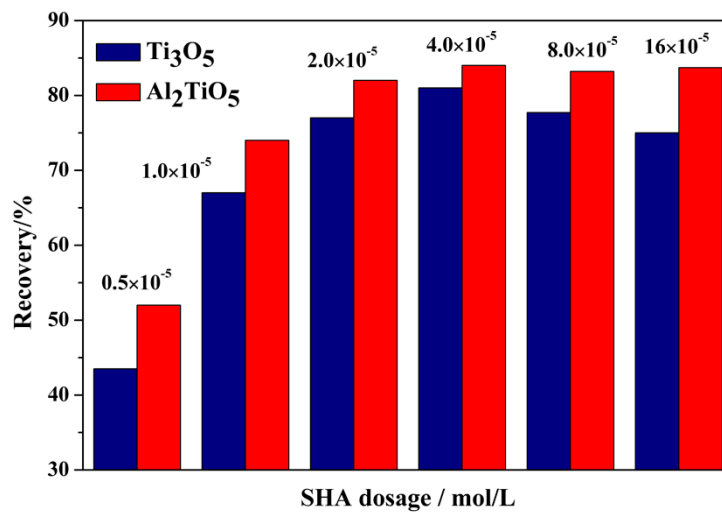
Figure 7. Dosage effect of SHA on the Flotability of Ti_3O_5 and Al_2TiO_5 crystals (pH = 7).

4. Conclusions

In this paper, DFT is used to study the effects of Al on anosovite crystal structure, electronic structure, and flotation behavior. Moreover, the flotation experiment on Ti_3O_5 and Al_2TiO_5 crystals are conducted, and DFT calculation results are accurate. The main conclusions are as follows:

(1) The energy of all Al_2TiO_5 band increased about 2 eV compared with that of Ti_3O_5, indicating that the valence and conduction bands have increased in energy. The energy band shifts to the positive direction promotes the flotation effect.

(2) Compared with Ti_3O_5 crystal, O atom obtains more electrons in Al_2TiO_5 crystal because the Ti atom receives electrons more easily than Al atoms in the Al_2TiO_5 crystal. The Al_2TiO_5 crystal possesses a larger Ti–O bond population than Ti_3O_5, and the Ti–O bonds length is shorter; therefore, the covalency of Al_2TiO_5 crystal is stronger. Moreover, the Al–O bonds covalency in the Al_2TiO_5 crystal is greater than that in the Ti_3O_5 crystal.

(3) The Al_2TiO_5 crystal has a higher recovery rate compared with the Ti_3O_5 crystal when the flotation conditions are the same. Therefore, doping an Al component into the Ti_3O_5 crystal should be beneficial for improving the flotation effect from TBBF slag.

Author Contributions: Conceptualization, S.R. and J.Y.; methodology, S.R.; software, Y.S.; validation, Z.S., W.L. and X.L.; formal analysis, Z.S.; investigation, Z.S.; resources, Y.S.; data curation, Y.S.; writing—original draft preparation, Z.S.; writing—review and editing, Z.S.; visualization, W.L.; supervision, S.R.; project administration, S.R.; funding acquisition, S.R. All authors have read and agreed to the published version of the manuscript.

Conflicts of Interest: The authors declare no conflict of interest.

References

1. Xiong, Y.; Aldahri, T.; Liu, W.; Chu, G.; Zhang, G.; Luo, D.; Yue, H.; Liang, B.; Li, C. Simultaneous preparation of TiO_2 and ammonium alum, and microporous SiO_2 during the mineral carbonation of titanium-bearing blast furnace slag. *Chin. J. Chem. Eng.* **2020**. [CrossRef]
2. Wang, L.; Liu, W.; Hu, J.; Liu, Q.; Yue, H.; Liang, B.; Zhang, G.; Luo, D.; Xie, H.; Li, C. Indirect mineral carbonation of titanium-bearing blast furnace slag coupled with recovery of TiO_2 and Al_2O_3. *Chin. J. Chem. Eng.* **2018**, *26*, 583–592. [CrossRef]
3. Gao, J.; Li, C.; Liu, W.; Hu, J.; Wang, L.; Liu, Q.; Liang, B.; Yue, H.; Zhang, G.; Luo, D.; et al. Process simulation and energy integration in the mineral carbonation of blast furnace slag. *Chin. J. Chem. Eng.* **2019**, *27*, 157–167. [CrossRef]

4.   Li, J.; Zhang, Z.; Zhang, M.; Guo, M.; Wang, X. The Influence of SiO_2 on the Extraction of Ti Element from Ti-bearing Blast Furnace Slag. *Steel Res Int.* **2011**, *82*, 607–614. [CrossRef]

5.   Zhang, L.; Zhang, L.; Wang, M.; Li, G.; Sui, Z. Dynamic oxidation of the Ti-bearing blast furnace slag. *ISIJ Int.* **2006**, *46*, 458–465. [CrossRef]

6.   Xia, Y.H.; Lou, T.P.; Sui, Z.T. Study on Micrographics of Perovskite Crystallization. *J. Northeastern Univ (Nat. Sci.).* **2001**, *22*, 307–310.

7.   Guo, P.; Zhao, P. Technical analysis on selective separation and enrichment of Ti-bearing blast furance slag based on phase diagrams. *Iron Steel Vanad. Titan.* **2005**, *26*, 5–10.

8.   Xu, C.; Yuan, Z.; Wang, X. Preparation of TiCl4 with the Titanium Slag Containing Magnesia and Calcia in a Combined Fluidized Bed. *Chin. J. Chem. Eng.* **2006**, *14*, 281–288. [CrossRef]

9.   Ren, S.; Zhang, J.L.; Wu, L.S.; Su, B.X.; Xing, X.D.; Zhu, G.Y. Effect of TiO_2 on equilibrium phase sinter at oxygen partial pressure of 5×10^{-3} atm. *Ironmak. Steelmak.* **2014**, *41*, 132–137. [CrossRef]

10. Ren, S.; Zhang, J.L.; Xing, X.D.; Su, B.X.; Wang, Z.; Yan, B.J. Effect of B2O3 on phase compositions of high Ti bearing titanomagnetite sinter. *Ironmak. Steelmak.* **2013**, *41*, 500–506. [CrossRef]

11. Ren, S.; Zhang, J.; Wu, L.; Liu, W.; Bai, Y.; Xing, X.; Su, B.; Kong, D. Influence of B2O3 on Viscosity of High Ti-bearing Blast Furnace Slag. *ISIJ Int.* **2012**, *52*, 984–991. [CrossRef]

12. Ren, S.; Liu, Q.C.; Zhang, J.L.; Chen, M.; Ma, X.; Zhao, B. Laboratory study of phase transitions and mechanism of reduction of FeO from high Ti-bearing blast furnace primary slag by graphite. *Ironmak. Steelmak.* **2014**, *42*, 117–125. [CrossRef]

13. Ren, S.; Zhang, J.L.; Liu, Q.C.; Chen, M.; Ma, X.; Li, K.J.; Zhao, B. Effect of B_2O_3 on reduction of FeO in Ti bearing blast furnace primary slag. *Ironmak. Steelmak.* **2014**, *42*, 498–503. [CrossRef]

14. Ren, S.; Zhao, Q.; Yao, L.; Liu, Q. Precipitation behavior of perovskite and anosovite crystals from high Ti-bearing blast furnace slag with small amount of B2O3. *CrystEngComm* **2016**, *18*, 1393–1402. [CrossRef]

15. Ren, S.; Guo, F.; Zhou, J.; Yang, J.; Yao, L.; Kong, M. Effect of compositions and additives content on crystallization behavior of Ti-rich phase from Ti-bearing blast furnace slag. *Met. Res. Technol.* **2017**, *114*, 415. [CrossRef]

16. Ren, S.; Zhang, J.L.; Liu, Q.C.; Li, K.J.; Zhao, B. Precipitation kinetics of anosovite in modified high Ti-bearing blast furnace slag. *Metall. Res. Technol.* **2015**, *112*, 105. [CrossRef]

17. Zhao, C.-H.; Wu, B.-Z.; Chen, J. Electronic structure and flotation behavior of monoclinic and hexagonal pyrrhotite. *J. Central South Univ.* **2015**, *22*, 466–471. [CrossRef]

18. He, G.-C.; Xiang, H.-M.; Jiang, W.; Kang, Q.; Chen, J.-H. First-principles theory on electronic structure and floatability of spodumene. *Rare Met.* **2014**, *33*, 742–748. [CrossRef]

19. Wang, Y.-J.; Wen, S.-M.; Feng, Q.-C.; Liu, J.; Ren, W.-C. Effects of magnesium and cooling rate on titanium phase transformation for production of TiO_2. *Trans. Nonferrous Met. Soc. China* **2016**, *26*, 2518–2522. [CrossRef]

20. Cohen, A.J.; Mori-Sánchez, P.; Yang, W. Insights into Current Limitations of Density Functional Theory. *Sci.* **2008**, *321*, 792–794. [CrossRef]

21. Geerlings, P.; De Proft, F.; Langenaeker, W. Conceptual density functional theory. *Chem. Rev.* **2003**, *103*, 1793–1874. [CrossRef] [PubMed]

22. Li, K.; Zhao, Y.-L.; Zhang, P.; He, C.; Deng, J.; Ding, S.; Shi, W. Combined DFT and XPS investigation of iodine anions adsorption on the sulfur terminated (001) chalcopyrite surface. *Appl. Surf. Sci.* **2016**, *390*, 412–421. [CrossRef]

23. Wang, Y.; Xian, Y.; Wen, S.; Deng, J.; Wu, D. The electronic structures of magnesium-bearing anosovite ($Mg_n Ti_{3-n} O_5$ $0 \leq n \leq 1$) and its response to flotation. *J. Alloy Compd.* **2017**, *708*, 982–988. [CrossRef]

24. Clark, S.J.; Segall, M.D.; Pickard, C.J.; Hasnip, P.J.; Probert, M.I.J.; Refson, K.; Payne, M.C. First principles methods using CASTEP. *Zeitschrift für Kristallographie - Crystalline Materials* **2005**, *220*, 567–570. [CrossRef]

25. Dassault Systèmes BIOVIA. *Materials Studio v2016*; Dassault Systèmes: San Diego, CA, USA, 2016.

26. Kresse, G.; Joubert, D. From ultrasoft pseudopotentials to the projector augmented-wave method. *Phys. Rev. B* **1999**, *59*, 1758–1775. [CrossRef]

27. Mele, E.J.; Ritsko, J.J. Fermi-level lowering and the core exciton spectrum of intercalated graphite. *Phys. Rev. Lett.* **1979**, *43*, 68–71. [CrossRef]

28. Zhang, L.; Gao, Y. Summarization of relation between surface properties and Floatability of minerals. *Gold J.* **2000**, *1*, 30–33.

29. Carta, M.; Ciccu, R.; Del Fa, C.; Ferrara, G.; Ghiani, M.; Massacci, P. The influence of the structure of mineral surface energy on electric separation and flotation. *Proc. IX IMPC* **1970**, *4*, 47–57.

30. Mulliken, R.S. Electronic Population Analysis on LCAO–MO Molecular Wave Functions. I. *J. Chem. Phys.* **1955**, *23*, 1833–1840. [CrossRef]

31. Mulliken, R.S. Electronic Population Analysis on LCAO–MO Molecular Wave Functions. II. Overlap Populations, Bond Orders, and Covalent Bond Energies. *J. Chem. Phys.* **1955**, *23*, 1841–1846. [CrossRef]

32. Mulliken, R.S. Electronic population analysis on LCAO-MO molecular wave functions. III. effects of hybridization on overlap and gross AO populations. *J. Chem. Phys.* **1955**, *23*, 2338–2342. [CrossRef]

33. Mulliken, R.S. Electronic Population Analysis on LCAO-MO Molecular Wave Functions. IV. Bonding and Antibonding in LCAO and Valence-Bond Theories. *J. Chem. Phys.* **1955**, *23*, 2343–2346. [CrossRef]

34. Wang, X.-F.; Wang, Y.-J.; Wen, S.-M.; Yin, P.-G. Flotation behavior and adsorption mechanism of salicylhydroxamic acid in artificial mineral anosovite. *J. Central South Univ.* **2019**, *26*, 806–812. [CrossRef]